Interfacial properties of $LaMnO_3/LaNiO_3$ superlattices grown along (001) and (111) orientations

C. Piamonteze,[1] M. Gibert,[2] J. Heidler,[1] J. Dreiser,[1] S. Rusponi,[3] H. Brune,[3] J.-M. Triscone,[2] F. Nolting,[1] and U. Staub[1]

[1]*Swiss Light Source, Paul Scherrer Institut, CH-5232 Villigen PSI, Switzerland*

[2]*Department of Quantum Matter Physics, University of Geneva, 24 Quai Ernest-Ansermet, 1211 Geneva, Switzerland*

[3]*Institute of Condensed Matter Physics, École Polytechnique Fédérale de Lausanne, CH-1015 Lausanne, Switzerland*

(Received 10 February 2015; revised manuscript received 20 May 2015; published 29 July 2015)

We have employed x-ray absorption spectroscopy and x-ray magnetic circular dichroism (XMCD) at the Ni and Mn $L_{3,2}$ edges in $LaMnO_3/LaNiO_3$ superlattices grown along (001) and (111) orientations. Our results show a significant XMCD signal and thus the presence of magnetic moments localized on both Ni and Mn, which are ferromagnetically coupled to each other. X-ray absorption experiments reveal a charge transfer between Ni and Mn which is larger for (111) than for (001) superlattices. These results are compared to theoretical predictions for such superlattices.

DOI: 10.1103/PhysRevB.92.014426 PACS number(s): 73.21.Cd, 75.47.Lx, 75.70.Cn, 78.70.Dm

I. INTRODUCTION

Transition-metal oxides exhibit a wide variety of remarkable properties such as high-temperature superconductivity, metal-insulator transitions, colossal magnetoresistance, and, more recently studied, magnetoelectric coupling. These properties result from the strong correlation between structural, orbital, and magnetic degrees of freedom. For this reason, transition-metal oxides have long been a major focus of condensed-matter research, and the search for systems with new or enhanced functionalities continues to be highly motivated. One way of tailoring such properties is by constructing artificial systems through the deposition of superlattices [1,2]. In heterostructures, the interface between two dissimilar materials can lead to properties not present in the component materials, for example, ferromagnetism at the interface between an antiferromagnet and a paramagnet [3] or the two-dimensional electron gas observed at the interface of insulators $LaAlO_3$ and $SrTiO_3$, one of the most heavily studied heterostructures to date [4]. Recently, an interesting exchange bias (EB) effect has been observed in superlattices of $LaMnO_3/LaNiO_3$ (LMO/LNO) grown along the cubic perovskite (111) direction [5]. The EB disappears above 30 K, and it is not observed for superlattices grown along (001). The exchange bias effect has been known for a long time in ferromagnetic/antiferromagnetic heterostructures [6]. It is surprising, however, that such an effect is observed in superlattices of LMO and LNO since these systems are antiferromagnetic and paramagnetic in bulk, respectively.

Manganites are widely studied systems, the most famous compounds being $La_{1-x}Sr_xMnO_3$ and $Pr_{1-x}Ca_xMnO_3$. The interest in these systems is primarily due to the colossal magnetoresistance observed at certain doping values, which is associated with a metal-insulator transition driven by ferromagnetic ordering. Another interesting aspect of these systems is the flexibility to tailor the magnetic and transport properties by electron doping or strain [7,8]. $LaMnO_3$ is an antiferromagnetic insulator in bulk, but in thin films it often exhibits ferromagnetism, mostly due to strain imposed by the substrate. $LaNiO_3$ is a paramagnetic metal, but all other members of the nickelate family with smaller lanthanide ions exhibit a metal-insulator transition as a function of temperature [9] and an antiferromagnetic ordering [10]. A metal-insulator transition has also been observed in ultrathin LNO films as a function of thickness [11]. Angle-resolved photoemission measurements of *in situ* prepared films (through molecular beam epitaxy) show a sharp metal-to-insulator transition upon reducing the thickness from 3 to 2 unit cells [12]. In superlattices of $LaNiO_3/LaAlO_3$, a second-order metal-insulator transition and antiferromagnetic ordering were observed for bilayers with only a two-unit-cell-thick $LaNiO_3$ layer, while those with four-unit-cell thickness did not exhibit such phase transitions [13]. In these superlattices the role of the interface has been evidenced by x-ray linear dichroism and x-ray reflectivity, which showed a larger orbital occupation anisotropy at the interface compared to the inner layers [14].

A few experimental investigations have explored heterostructures combining manganites and nickelates [5,15–21]. Ferromagnetism that is present only at the interface between $LaNiO_3$ and $CaMnO_3$ has been observed by x-ray magnetic circular dichroism combined with polarized neutron reflectometry [16]. Exchange bias has been observed in bilayers of $La_{0.75}Sr_{0.25}MnO_3$ and $LaNiO_3$ [18] (LSMO/LNO) grown along (001) direction.

There were two main theoretical publications following the discovery of the EB effect in LMO/LNO superlattices by Gibert *et al.* [5]. Using tight-binding calculations, Dong and Dagotto [22] compared three different superlattice orientations and found very little magnetization in the Ni layers for (001) compared to the (111) orientation. The enhanced magnetism in the Ni layers of (111)-oriented superlattices is attributed to quantum confinement of the Ni spin-down bands, which is most effective for this orientation. Lee and Han [23], on the other hand, found a considerable induced magnetic moment in (001) stacking and concluded that the induced magnetic moment on Ni is proportional to the charge transfer between Ni and Mn at the interface. Indeed, for (001) superlattices large charge transfer has been observed [19].

Here, we use x-ray absorption spectroscopy (XAS) and x-ray magnetic circular dichroism (XMCD) as elemental probes of the electronic and magnetic properties of (001) and (111) oriented LMO/LNO superlattices of different periodicities. We observe a ferromagnetic coupling between Ni and Mn. Our results also suggest that different types of magnetic ions, which could be antiferromagnetic or paramagnetic, coexist with those ferromagnetically coupled. A larger charge transfer is found for (111) superlattices compared to (001).

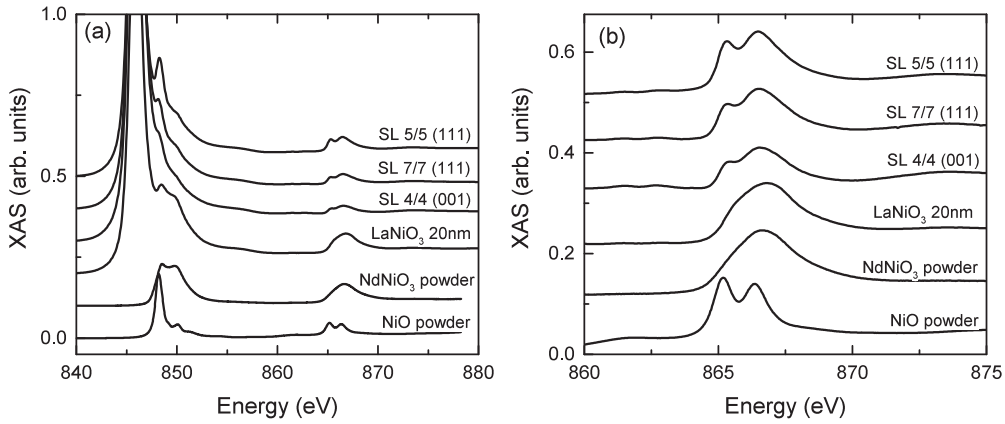

FIG. 1. XAS measured at (a) La M_4 (846 eV), Ni L_3 (849 eV), and Ni L_2 (866 eV) edges and (b) only the Ni L_2 edge region. Spectra are vertically offset for better visualization.

II. MATERIALS AND EXPERIMENT

LMO/LNO superlattices (SLs) were grown on $SrTiO_3$ (STO) substrates by off-axis magnetron sputtering. Details on sample preparation and typical structural characterization can be found in Ref. [5]. All superlattices studied here have a terminating top layer of $LaMnO_3$. Three periodicities and two crystallographic directions were measured. The periodicities given here correspond to the number of layers along a particular direction, and in each case the number of repetitions was adjusted to achieve a total thickness of around 45 nm. It should be noted that the same number of layers along different growth directions will result in different total thicknesses since the metal-metal planar distance is around 2.2 Å for (111) and 3.84 Å for (001) orientation. For SLs grown on STO(111) two periodicities were measured: 5/5 and 7/7. The 7/7 SL was grown in exactly the same conditions as the one published in Ref. [5], exhibiting equally good x-ray diffraction and equivalent EB. For SLs grown on STO(001), a 4/4 periodicity was measured. Throughout the paper, the SLs are identified by the periodicity and growth direction as 5/5(111), 7/7(111), and 4/4(001). Twenty-nanometer-thick films of LMO and LNO grown on STO(111) were also measured under the same conditions for comparison, along with powder samples of $NdNiO_3$ and NiO.

X-ray absorption measurements were performed at the X-Treme beamline [24] at the Swiss Light Source. The spectra were acquired by measuring the total electron yield (TEY) at 2 K, various applied magnetic fields, and an incidence angle (the angle between the x-ray beam direction and the sample normal) of 60°. The XAS curves shown are obtained as the sum of spectra measured with left and right circular polarization. The XMCD is defined as the difference between spectra measured with left and right circular polarization. The beamline is equipped with an elliptically polarizing undulator delivering photons with a $\geqslant$98% degree of circular polarization. Therefore, for the sum-rule calculations, there is no need to correct for the degree of circular polarization. Magnetic measurements were carried out in a commercial superconducting quantum interference device (SQUID) magnetometer with the magnetic field applied parallel to the plane of the sample.

The multiplet calculation for Ni^{2+} XMCD shown in Fig. 4(a) was performed as described in Ref. [25].

III. RESULTS

A. X-ray absorption spectroscopy and charge transfer

Figure 1(a) shows the XAS measured at Ni $L_{3,2}$ edges for three SLs, 5/5(111), 7/7(111), and 4/4(001), and the following samples for comparison: $NdNiO_3$ powder, NiO powder, and a 20-nm $LaNiO_3$ thin film grown on STO(111). In Fig. 1(a) we see that the La M_4 edge (at 846 eV) overlaps partially with the Ni L_3 edge (at 849 eV), limiting the analysis in this region. Comparing the spectra measured for the $LaNiO_3$ thin film with the $NdNiO_3$ powder, we see that both show the double-feature characteristic of Ni^{3+} spectra in the metallic phase [26,27] at the Ni L_3 edge. Note that the valence Ni states considered throughout the paper correspond to nominal valence values. In the spectra measured for the SLs, this feature is not as pronounced, and the single strong peak of 5/5(111) more closely resembles the NiO spectrum. The fact that the $LaNiO_3$ thin film shows clear Ni^{3+} features is evidence that the differences observed in the SLs come from the interface with LMO.

In Fig. 1(b) we compare the Ni L_2-edge region for the different samples. This region has no overlap with La edges and shows quite distinct features between Ni^{3+} and Ni^{2+}. The differences between the SLs and the reference samples becomes clearer in this figure. All SLs show a double feature at the Ni L_2 edge, characteristic of Ni^{2+}, but they are by far not as well defined as in NiO, providing evidence of an additional contribution from Ni^{3+}. By comparing the spectral features among the three SLs, the one showing spectral features most similar to those of Ni^{2+} is the 5/5(111).

Complementing the information obtained at the Ni L edge, we plot in Fig. 2 the Mn XAS measured at Mn $L_{3,2}$ edges. The spectra for the SLs are compared to a 20-nm-thick $LaMnO_3$ thin film grown along the (111) direction. From published spectra of Mn XAS on $La_{1-x}Sr_xMnO_3$ [28] we know that more Mn^{4+} character leads to a shift of the XAS spectrum towards higher energies. Comparing the published spectra [28] with our data, we see that the spectrum for 5/5(111) clearly shows more Mn^{4+} character than the other SLs, while the Mn spectral features for 7/7(111) and 4/4(001) indicate a valence state between those of $LaMnO_3$ and the 5/5(111) SL.

From the XAS spectra we can conclude that the SL with Ni spectral features resembling more Ni^{2+} also shows more

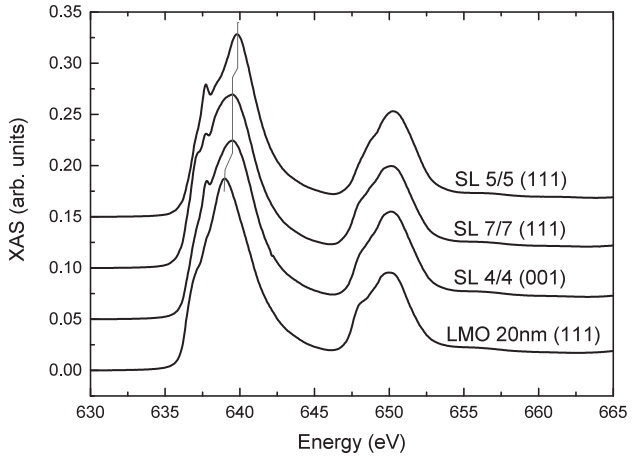

FIG. 2. XAS measured at Mn $L_{3,2}$ edges. The vertical line marks the position of the XAS maxima. Spectra are vertically offset to allow better visualization.

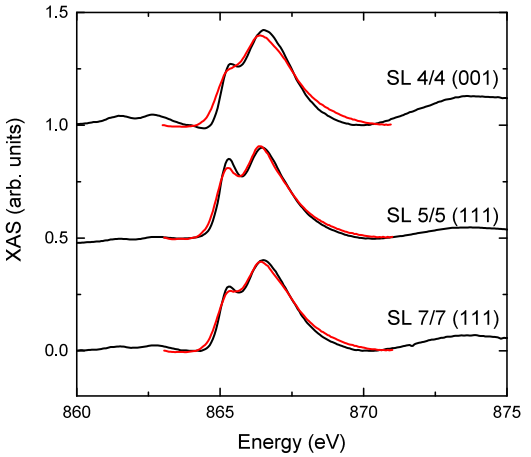

FIG. 3. (Color online) XAS measured at the Ni L_2 edge for the SLs (black line). Red lines are fits with a linear combination of the spectra measured for $NdNiO_3$ and NiO. Spectra are vertically offset for better visualization.

Mn^{4+} features, which indicates that a charge transfer between Ni and Mn occurs at the interface. This interpretation is also corroborated by the comparison of SLs grown along the (111) direction; the one with smaller periodicity (5/5) and therefore a larger ratio of interface layers to total number of layers shows a larger Ni^{2+}/Mn^{4+} contribution to the XAS than the SL with larger periodicity (7/7).

Since charge transfer (CT) seems to be an important ingredient in these SLs, we have attempted a quantitative analysis of the XAS to determine the amount of charge transfer between Ni and Mn. Because CT occurs at the interface, the measured spectra can be described by a superposition of two types of ions, the interface ions with large charge transfer with a spectral shape close to Ni^{2+} and Mn^{4+} and the center or top layers where the nominal valence (Ni^{3+}, Mn^{3+}) is mostly preserved. We have used a linear combination of the measured spectra of the two powder compounds, $NdNiO_3$ (Ni^{3+}) and NiO (Ni^{2+}), to fit the SL spectra measured at the Ni L_2 edge, which is undisturbed by the La M_4-edge contribution. It should be pointed out that while the assumption that center ions have a spectrum close to $NdNiO_3$ is quite reasonable, the spectral shape for the interface ions might deviate from that of a total charge transfer to Ni^{2+}. However, for simplicity, we assume here that the interface atoms have the same spectral features as Ni^{2+}.

The comparison between data and the fitting using the two measured spectra of the standard powder samples is shown in Fig. 3. The amount of Ni^{2+} character found is summarized in Table I. The 5/5(111) SL shows a much larger charge transfer than 7/7(111), as already expected from the spectral shape, while 4/4(001) is the SL with smallest amount of charge transfer among all three. The values obtained for the (111) SLs are, within error, identical to the value expected by making the simple assumption of one layer at the interface reduced to Ni^{2+}, while for 4/4(001) the value obtained is about half that expected by making the same assumption. It should be pointed out that four layers along (001) have approximately the same thickness as seven layers along (111); therefore, the differences observed cannot be attributed to the limited probing depth of TEY with an electron escape depth in the range of 30 to 50 Å [29].

B. X-ray magnetic circular dichroism and magnetic properties

Figures 4(a) and 4(b) present the measured XMCD at the Ni and Mn L edges, respectively. The region just before the Ni L_3 edge corresponds to the La M_4 edge, which, although noisy, does not show an XMCD signal. In Fig. 4(a) a simulation of a Ni^{2+} XMCD spectra is plotted for comparison. The simulation was done using ligand-field multiplet theory with the parameters published elsewhere [25].

There are a few important aspects to point out in these figures. The first is that Ni shows a clear XMCD signal for both (111) and (001) stackings. As expected, the thin film of $LaNiO_3$ shows no XMCD. The second point to notice is that the XMCD has the same sign for both Mn and Ni, demonstrating a ferromagnetic alignment between the two ions. Among the different samples, the only remarkable difference in the Ni XMCD is in its intensity. The Ni XMCD spectral shape remains mostly the same for all SLs, which in turn is very similar to a Ni^{2+} XMCD spectrum, as can be seen by comparison with the simulated spectrum plotted in Fig. 4(a). On the other hand, the Mn XMCD spectral shape shown in Fig. 4(b) changes among the different samples due to the different contributions of Mn^{3+} and Mn^{4+} to the XMCD spectra.

Sum rules [30–32] have been applied to both the Ni and Mn spectra. Correction factors for the effective spin sum rule due to $2p$-$3d$ multiplet effects have been calculated as described in

TABLE I. Amount of Ni^{2+} obtained from the linear combination fit of the XAS spectra and from the model discussed in the text.

Sample	XAS spectra[a]	expected[b]
5/5 (111)	42(5)%	40%
7/7 (111)	30(5)%	29%
4/4 (001)	23(5)%	50%

[a]From Fig. 3.
[b]Considering one layer at each interface reduced to Ni^{2+}.

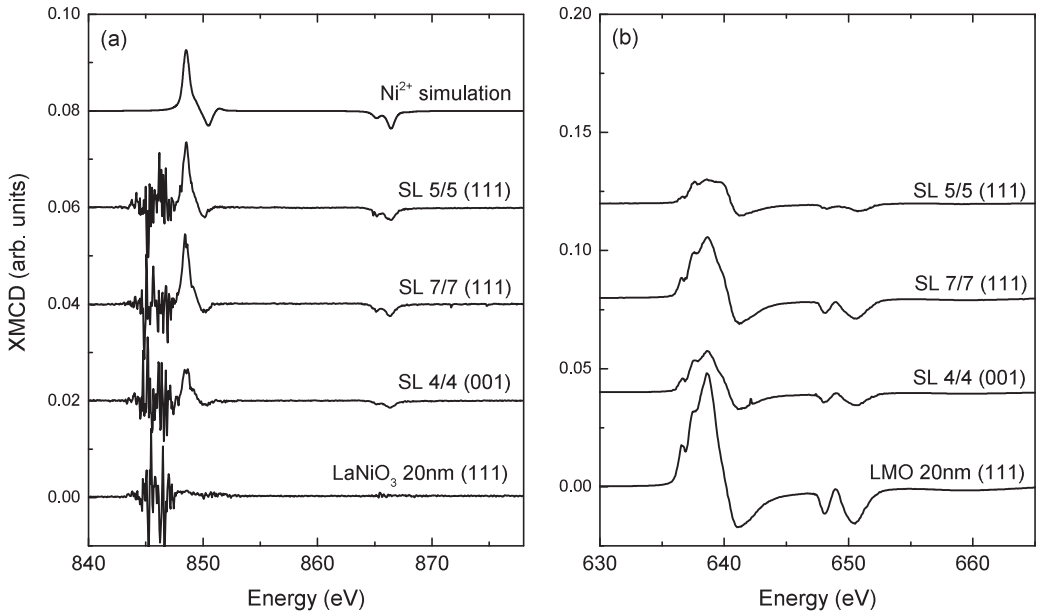

FIG. 4. XMCD spectra at (a) Ni and (b) Mn L edges measured at 0.5 T and 2 K. The XMCD data are scaled to the XAS spectra shown in Figs. 1(a) and 2. Spectra are vertically offset to allow better visualization.

Ref. [33]. The correction factors used were 1.1 and 1.7 for Ni and Mn, respectively. The number of holes used for Ni was 2.5, taken from charge-transfer ligand-field multiplet simulations for Ni^{3+} in nickelates [26,34]. For Mn we used 5.5 holes, which is found in cluster calculations for $LaMnO_3$ [35]. As pointed out previously, the charge transfer varies among the different SLs, so strictly speaking, the number of holes will also vary accordingly. The number of holes calculated from cluster calculations [35] for Ni^{2+} and Mn^{4+} is 1.8 and 6.4, respectively. If we were to use those numbers together with the amount of charge transfer found in Table I, the number of holes for Mn (Ni) in the SL would be 5.9 (2.2), 5.8 (2.3), and 5.7 (2.3) for 5/5(111), 7/7(111), and 4/4(001), respectively. The differences in calculated moments would be a 7%–8% larger moment for both Mn and Ni in the SLs. This difference is within the error bars; therefore, we have opted to keep the number of holes fixed between the different samples as a matter of simplicity. The La contribution to the XAS and the noisy region in the same energy range in the Ni XMCD makes the application of sum rules to the full Ni spectrum impossible. Therefore, the integration range for the Ni spectra starts at 847.7 eV. This reduced integration range can lead to an inaccurate moment estimate due to two effects: part of the Ni L_3-edge XAS might be excluded in the integration range and part of the La M_4-edge XAS might still be included. In order to estimate which effect is dominating and how large our error might be, we have used the data measured for $NdNiO_3$ and $LaMnO_3$ as references of pure Ni and pure La XAS, respectively. We find that the Ni XAS in the SLs is overestimated by about 8% compared to $NdNiO_3$ due to the inclusion of a small La contribution. This implies an equal relative underestimation of the Ni moment, which is within the error.

The sum-rule results for the total moment (spin plus orbital angular moments) $M = m_s + m_l$ for Ni and Mn are shown in Table II. The orbital moment is close to zero for all samples [36]. The LMO (111) thin-film moment measured by bulk magnetization is $3.6\mu_B$ [5], which is comparable to the value of $3.4\mu_B$ obtained by the sum-rule analysis. In comparison to LMO, all SLs have a smaller moment. However, one should be careful with this comparison since the presence of Mn^{4+} in the SLs would reduce the measured moment. The predicted moment for Mn^{4+} varies from $3.0\mu_B$ in La_2NiMnO_6 double perovskite [37] to $2.4\mu_B$ in $SrMnO_3$ [38]. In order to estimate the expected Mn moment in the SLs, we can use the amount of charge transfer given in Table I to weigh the Mn^{3+}/Mn^{4+} moments of $3.5\mu_B$ and $3.0\mu_B$, respectively. The expected moments thus obtained are in the range of $3.3\mu_B$ to

TABLE II. Total magnetic moment derived from XMCD sum rules. All values are in μ_B, and errors are given in parentheses. For more details on the number of holes and correction factors, see text.

	M_{Mn}		M_{Ni}		M_{Ni}/Ni^{2+} character	
Sample	0.5 T	6.0 T	0.5 T	6.0 T	0.5 T	6.0 T
5/5 (111)	0.82 (0.2)	2.23 (0.2)	0.13 (0.02)	0.20 (0.02)	0.31 (0.05)	0.46 (0.05)
7/7 (111)	2.07 (0.2)	3.15 (0.3)	0.13 (0.02)	0.13 (0.02)	0.43 (0.04)	0.43 (0.05)
4/4 (001)	1.30 (0.1)	2.40 (0.2)	0.06 (0.02)	0.12 (0.02)	0.24 (0.05)	0.51 (0.05)
LMO (111)	3.45 (0.3)					

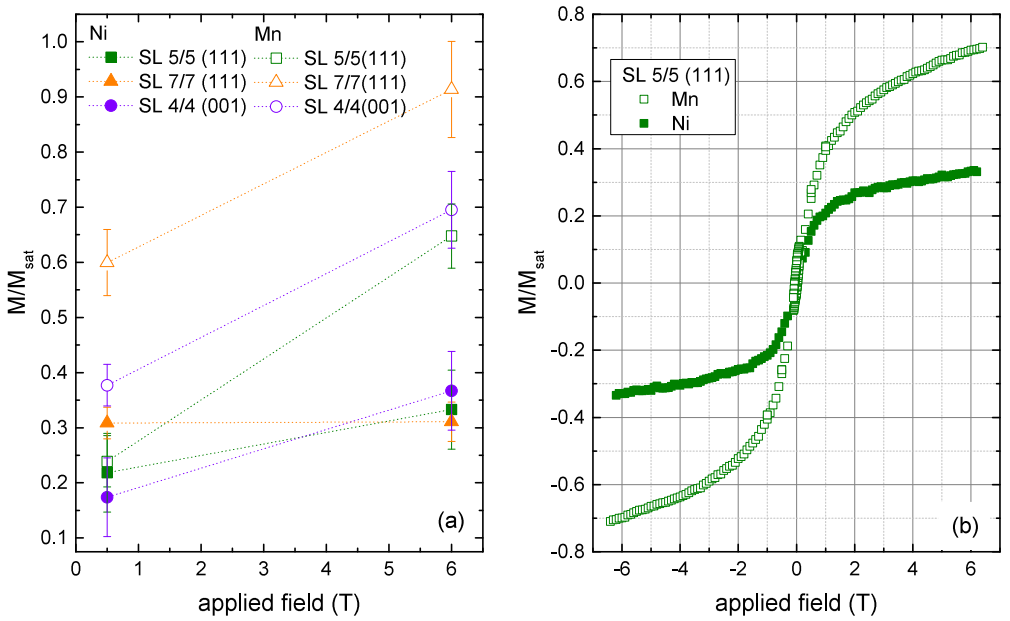

FIG. 5. (Color online) (a) Mn and Ni magnetic moments as a function of applied magnetic field for the three SLs. The total magnetization value for Mn and the rescaled Ni magnetization by the Ni^{2+} character (from Table II) have been divided by $3.45\mu_B$ and $1.4\mu_B$, respectively. The lines are guides to the eyes. (b) Mn and Ni magnetization curves measured for 5/5 (111) SL after zero-field cooling.

$3.4\mu_B$ for all three SLs and therefore are only slightly smaller than that for the LMO thin film. These expected values are still significantly larger than those measured in the 5/5(111) and 4/4(001) SLs, which vary between $0.8\mu_B$ and $1.3\mu_B$ at 0.5 T and $2.2\mu_B$ and $2.4\mu_B$ at 6.0 T. For 7/7(111) at 6.0 T the measured Mn moment of $3.15\mu_B$ is not too far from saturation.

As discussed previously, the Ni XMCD spectral shape indicates that only Ni^{2+} ions contribute to the XMCD. On the other hand, the sum rules will give the moment per Ni considering the total amount of Ni probed. Therefore, in the last column of Table II we have renormalized the Ni sum-rule results by the amount of Ni^{2+} character obtained in Table I. The rescaled sum-rule results for Ni vary in the range of $0.24\mu_B$ to $0.43\mu_B$ at 0.5 T and $0.43\mu_B$ to $0.51\mu_B$ at 6.0 T. Therefore, even after the rescaling, the Ni moments are only a fraction of the predicted moment of $1.4\mu_B$ in La_2NiMnO_6 double perovskite [37].

For a better graphical visualization of the sum rule results and their dependence on magnetic field we have plotted in Fig. 5(a) the measured Ni and Mn magnetic moment divided by the expected saturation value of $1.4\mu_B$ for Ni^{2+} and our measured value of $3.45\mu_B$ for Mn^{3+} in the LMO thin film. Interestingly, for 5/5(111) and 4/4(001) SLs the Ni and Mn moments measured at 6 T are significantly larger than those for 0.5 T, indicating that even at 0.5 T, which is far above the coercive field of about 10–100 mT, the sample is not completely saturated. For 7/7(111) the Mn moment still increases with the applied field above 0.5 T, while Ni is approximately the same. The increase of moment with applied field is also clearly seen in the magnetization curve for 5/5 (111) plotted in Fig. 5(b).

XMCD in remanence was also measured (not shown). For 7/7(111) SL we measure a moment of $0.7\mu_B$ for Mn and $0.05\mu_B$ for Ni. For 4/4(001) and 5/5(111) the remanent magnetization is very small, and sum rules are not reliable. By comparing the XMCD magnitude among the three SLs, we can estimate that for 4/4(001) the remanent moment for both Mn and Ni is approximately 8 times smaller than that measured for 7/7(111) in remanence, while for 5/5(111) the Mn moment is around 6 times smaller than for 7/7(111) in remanence and the Ni XMCD is almost within the noise.

In order to check if the T_c for both Ni and Mn are the same, we have measured the temperature dependence of the XMCD signal for both Mn and Ni in the 7/7(111) SL. The result is plotted in Fig. 6 and is compared to SQUID magnetometry measurements taken in the same sample under similar conditions. The XMCD signal was measured while

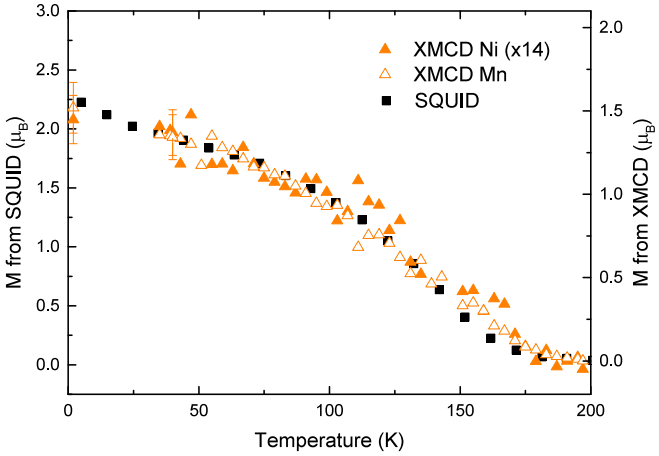

FIG. 6. (Color online) Temperature dependence of the Ni and Mn magnetization obtained from the XMCD signals. Measured under applied field of 75 mT after field cooling at 0.5 T. The XMCD result is compared to the SQUID magnetometry measured in the same sample under similar conditions.

slowly increasing the temperature. Spectra with better statistics at 2 and 40 K were measured in order to apply sum rules and scale the XMCD intensity curves at these points. The absolute uncertainty of the data in Fig. 6 corresponds to errors of the sum-rule calculation. The temperature dependence is very similar for Ni and Mn, demonstrating that they are coupled to each other and exhibit the same T_c. However, the value of the total magnetic moment obtained from XMCD is smaller than that measured by bulk magnetization. One possible explanation is that the magnetic moment in the upper layers of the SL is smaller than that in the bottom layers.

IV. DISCUSSION

Our XAS measurements show that for SLs along the (111) orientation an increased charge transfer is observed for the 5/5 (111) SL compared to 7/7 (111), which indicates that CT between Ni and Mn takes place at the interface, in agreement with theoretical models [22,23]. Significant charge transfer at the interface was also observed in LSMO/LNO [18] bilayers and in LMO/LNO SLs along (001) [19]. Therefore, it seems to be a universal effect that the nominal valences of Ni^{3+} and Mn^{3+} in LNO and LMO change to Ni^{2+}/Mn^{4+} when Ni and Mn are in the vicinity of each other. This result becomes clear in view of the Ni^{2+}/Mn^{4+} valence states found in La_2NiMnO_6 double perovskite [37,39]. As for the dependence of CT on the growth direction, the 7/7(111) and 4/4(001) SLs make a good comparison since their total layer thicknesses are approximately the same. Comparing these two SLs, we find that the CT obtained for the (001) orientation is smaller than that for (111) orientation (Table I), which is consistent with the reduced ratio of Mn-Ni/Mn-Mn (or Ni-Mn/Ni-Ni) nearest neighbors for the interfaces along (001) compared to those along (111), which is 1/5 and 3/3, respectively.

The charge-transfer values obtained are quite comparable to those predicted. For an LMO/LNO 2/4(001) SL, Lee and Han [23] calculated that the charge transferred to Ni is 0.26 electron. Dong and Dagotto [22] found that 0.3 electron is passed from Mn to Ni for a SL with two Ni layers, and this value is the same for all SL orientations. We find the transfer of 0.23(5) electron for 4/4(001), 0.42(5) electron for 5/5(111), and 0.3(5) electron for 7/7(111) (see Table I), in the same range as the predicted values.

As for magnetism, our results show that both Ni and Mn present a net magnetic moment, and for both (111) and (001) SLs the coupling of the net moment between these two ions is ferromagnetic, as expected from Goodenough-Kanamori rules for a Ni^{2+}-Mn^{4+} configuration [40]. This result is again similar to La_2NiMnO_6 double perovskite, for which ferromagnetic coupling between Ni^{2+} and Mn^{4+} due to superexchange is predicted and observed [37,39]. In addition, our results show that Ni and Mn have the same T_c and follow the same behavior of magnetization as a function of temperature, as seen in Fig. 6.

Here, we would like to discuss the quantitative agreement of the proposed models for the magnetic structure with our results. All models available in the literature [5,22,23] propose an oscillatory Ni magnetic structure, with antiparallel moments of decaying magnitude as the distance from the interface increases. X-ray absorption spectroscopy cannot give definite proof of this oscillatory structure. However, it is possible to compare the net moments measured here with those resulting from the proposed model. The other members of the nickelate family [10] exhibit true antiferromagnetic ordering. Such an ordered structure is, of course, stable in an applied field of 6 T, and therefore, no XMCD signal can be measured. For the existence of exchange bias, the presence of pinned moments at the interface, which do not rotate under a moderate applied field, would be expected, as proposed in the model of Gibert *et al.* [5]. It is not clear what the influence of the magnetic field would be in the models of Lee and Han [23] and Dong and Dagotto [22], namely, if the oscillatory Ni structure would be frozen or if the Ni moments would cant in the direction of the applied magnetic field. If the magnetic structure should be preserved, then none of the models can describe our results in terms of absolute values since the predicted net Ni moment per Ni atom is in the range of $0.02\mu_B$ and therefore is far too small compared to our results. On the other hand, the Ni moment at the interface layer is in the same range as the scaled Ni moment measured here and is ferromagnetically coupled to the Mn interface layer. For example, Lee and Han [23] found $0.3\mu_B$ to $0.4\mu_B$ for the Ni moment at the interface for a LMO_2/LNO_4(001) SL, and Dong and Dagotto [22] found $0.12\mu_B$ to $0.3\mu_B$ for the Ni moment at the interface of a (111) SL. In the model of Dong and Dagotto, the induced Ni moment for a (001) SL is $< 0.1\mu_B$; therefore, it is much smaller than for the (111) orientation. Comparing the Mn moment magnitude measured here with those predicted in the literature, the values we obtain for 5/5(111) and 4/4(001) are lower than predicted since all calculations find a moment for Mn [5,22,23] that is close to saturation.

We now turn our attention to the field dependence of the magnetic moment. For Mn, all SLs show an increase in the magnetic moment above 0.5 T, which is already far above the coercive field of 10–100 mT. At 6 T, the Mn moment in 7/7(111) is close to saturation, while for the 4/4(001) and 5/5(111) SLs it is still 70% from saturation. Moreover, the remanent moment for the 7/7(111) SL is considerably larger than that for the 5/5(111) and 4/4(001) SLs. These different behaviors at high field for SLs with small and large periodicities seem to indicate different behaviors for Mn moments at the interface compared to moments in the inner layers. Pinned Mn moments at the interface would explain the fact that the saturation moment is not achieved, but they would not explain the linear dependence on the field. It seems more likely that this linear dependence comes either from moments which are weakly antiferromagnetically coupled or from paramagnetic moments. Rojas Sánchez *et al.* [18] also found indications for different behaviors of interface ions versus inner ions in LSMO/LNO bilayers.

The behavior of the Ni moment as a function of field also shows some interesting results. In Fig. 5, it is observed that at 6.0 T the Ni moment is between 30% and 40% of saturation and therefore much lower than M/M_{sat} for Mn. Moreover, for 5/5(111) and 7/7(111), the Ni moment does not seem to change much between 0.5 and 6.0 T, which is also noticeably different than the result for Mn. Therefore, the Ni moment on the (111) SLs will never reach the moment of $1.4\mu_B$ predicted for Ni^{2+} in La_2NiMnO_6. There are a few possible explanations for this small moment. One possibility is that the Ni-induced magnetic moment at the interface is small in magnitude. But if

this moment is induced by Mn, it should also follow the same behavior as a function of applied field, which does not seem to be the case. The other possible explanation is that there could be canceled moments due to either a true antiferromagnetic (AF) coupling or disordered pinned moments. The oscillatory Ni structure proposed in the model of Gibert et al. [5] could also be the origin of these canceled Ni moments. On the other hand, the 4/4(001) SL exhibits a larger rate of increase of the Ni moment versus field. This indicates that the Ni moments are not very strongly pinned in the (001) SL and possibly have a larger component of paramagnetic or weakly coupled antiferromagnetic moments which are canted under applied field. Our results therefore suggest that in addition to Ni-Mn ferromagnetism at the interface, there is likely a Ni-Ni AF coupling or disordered pinned moments in the (111) SLs. For 4/4(001) SL there seems to be weak AF or paramagnetic Ni ions since this superlattice shows a linear increase of the Ni moment with field. The existence of canceled moments (coming either from strong AF coupling or pinned moments) in the (111) SL and not in the (001) could explain why the EB is observed in one orientation but not in the other.

The proposed mechanism for the origin of the Ni magnetism is somewhat different in the two most recently published models by Lee and Han [23] and Dong and Dagotto [22]. Lee and Han propose that the Ni moment is purely proportional to the charge transfer, while Dong and Dagotto predicts it is due to quantum confinement and therefore larger in the (111) SL than in the (001) SL and, moreover, independent of charge transfer. Our measurements at 0.5 T show that the Ni moments for 7/7(111) and 5/5(111) are larger than that for 4/4(001). At 0.5 T we also see no scaling of magnetic moment with charge transfer since the rescaled Ni moments plotted in Fig. 5(a) are different among the three SLs. These results seem to agree with the predictions from Dong and Dagotto. On the other hand, at 6.0 T when the moment for 4/4(001) is larger, the Ni moment scaled by the Ni^{2+} character is very similar for all SLs, showing that in this high-field regime the moments do not depend on the growth direction and scale with the CT, as proposed by Lee and Han. Therefore, at this stage we cannot say that a single model can completely explain all of our results. It rather seems that all of them have important contributions but some ingredients are still missing. For example, it would be interesting to know what the predicted field dependence of the Ni moments is for the different superlattices and also what the effect of the interface is on the Mn moments.

V. CONCLUSION

We have studied the charge transfer and magnetism of Mn and Ni for LMO/LNO SLs with different periodicities grown along the (001) and (111) directions. Our results show (i) clear charge transfer between Ni and Mn at the interface, (ii) increased charge transfer for (111) SL compared to (001), (iii) a clear ferromagnetic coupling governing the net magnetic moments of Ni and Mn, and (iv) an indication of the coexistence of another type of magnetic ion. For Mn there could be a coexistence of ferromagnetism with weakly AF or paramagnetic moments since a linear increase of magnetization in high applied field is observed. Similar behavior is observed for Ni in 4/4(001). For Ni in the (111) SL, the presence of strong AF coupling or disordered pinned moments would be consistent with the reduced moment measured. Even though some results agree well with theoretical predictions, there are still a few points that are not properly explained by the current models. We therefore hope that these results will help in further improving the current theoretical models available for describing the magnetic and electronic structures at the interface of these complex and interesting SLs.

ACKNOWLEDGMENTS

The x-ray absorption measurements were performed on the EPFL/PSI X-Treme beamline at the Swiss Light Source, Paul Scherrer Institut, Villigen, Switzerland. We acknowledge B. Watts for help in proofreading the manuscript. This work was supported by the Swiss National Science Foundation through the National Center of Competence in Research, Materials with Novel Electronic Properties, MaNEP, and Division II. The research leading to these results has received funding from the European Research Council under the European Union's Seventh Framework Programme (FP7/2007-2013)/ERC Grant Agreement No. 319286.

[1] P. Zubko, S. Gariglio, M. Gabay, P. Ghosez, and J.-M. Triscone, Annu. Rev. Condens. Matter Phys. **2**, 141 (2011).
[2] H. Y. Hwang, Y. Iwasa, M. Kawasaki, B. Keimer, N. Nagaosa, and Y. Tokura, Nat. Mater. **11**, 103 (2012).
[3] K. S. Takahashi, M. Kawasaki, and Y. Tokura, Appl. Phys. Lett. **79**, 1324 (2001).
[4] A. Ohtomo and H. Y. Hwang, Nature (London) **427**, 423 (2004).
[5] M. Gibert, P. Zubko, R. Scherwitzl, J. Iniguez, and J.-M. Triscone, Nat. Mater. **11**, 195 (2012).
[6] J. Nogués and I. K. Schultz, J. Magn. Magn. Mater. **192**, 203 (1999).
[7] A.-M. Haghiri-Gosnet and J.-P. Renard, J. Phys. D **36**, R127 (2003).
[8] J. M. D. Coey, M. Viret, and S. von Molnár, Adv. Phys. **48**, 167 (1999).
[9] P. Lacorre, J. B. Torrance, J. Pannetier, A. I. Nazzal, P. W. Wang, and T. C. Huang, J. Solid State Chem. **91**, 225 (1991).
[10] J. L. García-Muñoz, J. Rodríguez-Carvajal, and P. Lacorre, Phys. Rev. B **50**, 978 (1994).
[11] R. Scherwitzl, S. Gariglio, M. Gabay, P. Zubko, M. Gibert, and J. M. Triscone, Phys. Rev. Lett. **106**, 246403 (2011).
[12] P. D. C. King, H. I. Wei, Y. F. Nie, M. Uchida, C. Adamo, S. Zhu, X. He, I. Božović, D. G. Schlom, and K. M. Shen, Nat. Nanotechnol. **9**, 443 (2014).
[13] A. V. Boris, Y. Matiks, E. Benckiser, A. Frano, P. Popovich, V. Hinkov, P. Wochner, M. Castro-Colin, E. Detemple, V. K. Malik, C. Bernhard, T. Prokscha, A. Suter, Z. Salman, E. Morenzoni, G. Cristiani, H. U. Habermeier, and B. Keimer, Science **332**, 937 (2011).
[14] E. Benckiser, M. W. Haverkort, S. Brück, E. Goering, S. Macke, A. Frañó, X. Yang, O. K. Andersen, G. Cristiani, H.-U.

Habermeier, A. V. Boris, I. Zegkinoglou, P. Wochner, H.-J. Kim, V. Hinkov, and B. Keimer, Nat. Mater. **10**, 189 (2011).
[15] K. R. Nikolaev, A. Bhattacharya, P. A. Kraus, V. A. Vas'ko, W. K. Cooley, and A. M. Goldman, Appl. Phys. Lett. **75**, 118 (1999).
[16] A. J. Grutter, H. Yang, B. J. Kirby, M. R. Fitzsimmons, J. A. Aguiar, N. D. Browning, C. A. Jenkins, E. Arenholz, V. V. Mehta, U. S. Alaan, and Y. Suzuki, Phys. Rev. Lett. **111**, 087202 (2013).
[17] P. Pandey, R. Rana, S. Tripathi, and D. S. Rana, Appl. Phys. Lett. **103**, 032403 (2013).
[18] J. C. Rojas Sánchez, B. Nelson-Cheeseman, M. Granada, E. Arenholz, and L. B. Steren, Phys. Rev. B **85**, 094427 (2012).
[19] J. Hoffman, I. C. Tung, B. B. Nelson-Cheeseman, M. Liu, J. W. Freeland, and A. Bhattacharya, Phys. Rev. B **88**, 144411 (2013).
[20] H. Tanaka, N. Okawa, and T. Kawai, Solid State Commun. **110**, 191 (1999).
[21] M. A. Novojilov, O. Y. Gorbenko, I. V. Nikulin, I. E. Graboy, A. R. Kaul, N. A. Babushkina, and L. M. Belova, Int. J. Inorg. Mater. **3**, 1165 (2001).
[22] S. Dong and E. Dagotto, Phys. Rev. B **87**, 195116 (2013).
[23] A. T. Lee and M. J. Han, Phys. Rev. B **88**, 035126 (2013).
[24] C. Piamonteze, U. Flechsig, S. Rusponi, J. Dreiser, J. Heidler, M. Schmidt, R. Wetter, M. Calvi, T. Schmidt, H. Pruchova, J. Krempasky, C. Quitmann, H. Brune, and F. Nolting, J. Synchrotron Radiat. **19**, 661 (2012).
[25] G. van der Laan, C. M. B. Henderson, R. A. D. Pattrick, S. S. Dhesi, P. F. Schofield, E. Dudzik, and D. J. Vaughan, Phys. Rev. B **59**, 4314 (1999).
[26] C. Piamonteze, F. M. F. de Groot, H. C. N. Tolentino, A. Y. Ramos, N. E. Massa, J. A. Alonso, and M. J. Martínez-Lope, Phys. Rev. B **71**, 020406(R) (2005).
[27] M. Medarde, A. Fontaine, J. L. García-Muñoz, J. Rodríguez-Carvajal, M. De Santis, M. Sacchi, G. Rossi, and P. Lacorre, Phys. Rev. B **46**, 14975 (1992).
[28] M. Abbate, F. M. F. de Groot, J. C. Fuggle, A. Fujimori, O. Strebel, F. Lopez, M. Domke, G. Kaindl, G. A. Sawatzky, M. Takano, Y. Takeda, H. Eisaki, and S. Uchida, Phys. Rev. B **46**, 4511 (1992).
[29] T. J. Regan, H. Ohldag, C. Stamm, F. Nolting, J. Lüning, J. Stöhr, and R. L. White, Phys. Rev. B **64**, 214422 (2001).
[30] B. T. Thole, P. Carra, F. Sette, and G. van der Laan, Phys. Rev. Lett. **68**, 1943 (1992).
[31] P. Carra, B. T. Thole, M. Altarelli, and X. Wang, Phys. Rev. Lett. **70**, 694 (1993).
[32] J. Stöhr, J. Electron Spectrosc. Relat. Phenom. **75**, 253 (1995).
[33] C. Piamonteze, P. Miedema, and F. M. F. de Groot, Phys. Rev. B **80**, 184410 (2009).
[34] V. Scagnoli, U. Staub, A. M. Mulders, M. Janousch, G. I. Meijer, G. Hammerl, J. M. Tonnerre, and N. Stojic, Phys. Rev. B **73**, 100409(R) (2006).
[35] T. Saitoh, A. E. Bocquet, T. Mizokawa, and A. Fujimori, Phys. Rev. B **52**, 7934 (1995).
[36] m_l for the 5/5(111), 7/7(111), and 4/4(001) SLs are, respectively, 0.03(9), 0.03(3), and 0.005(10) for Mn at 0.5 T; −0.004(17), 0.007(7), and 0.02(5) for Mn at 6.0 T; 0.01(1), 0.028(8), and 0.011(7) for Ni at 0.5 T; and 0.032(5), 0.015(5), and 0.02(3) for Ni at 6 T. For Mn in the LMO thin film at 0.5 T $m_l = 0.007(5)$.
[37] H. Das, U. V. Waghmare, T. Saha-Dasgupta, and D. D. Sarma, Phys. Rev. Lett. **100**, 186402 (2008).
[38] O. Chmaissem, B. Dabrowski, S. Kolesnik, J. Mais, J. D. Jorgensen, and S. Short, Phys. Rev. B **67**, 094431 (2003).
[39] H. Guo, A. Gupta, M. Varela, S. Pennycook, and J. Zhang, Phys. Rev. B **79**, 172402 (2009).
[40] J. B. Goodenough, *Magnetism and the Chemical Bond* (Interscience, New York, 1963).